Title

Mathematical modelling of the maternal cardiovascular system in the three stages of pregnancy

Authors

Chiara Corsini[1], Elena Cervi[2], Francesco Migliavacca[1], Silvia Schievano[2], Tain-Yen Hsia[2], and Giancarlo Pennati[1]

Affiliations

[1] Laboratory of Biological Structure Mechanics, Department of Chemistry, Materials and Chemical Engineering "Giulio Natta", Politecnico di Milano, Milan, Italy

[2] UCL Institute of Cardiovascular Science and Great Ormond Street Hospital for Children, NHS Foundation Trust, London, UK

Corresponding author

Chiara Corsini, PhD
Politecnico di Milano
Piazza Leonardo da Vinci, 32
20133 Milan, Italy
Tel: +39 02 2399 4283
chiara.corsini@polimi.it

Abstract

In this study, a mathematical model of the woman circulation during pregnancy is presented in order to investigate the hemodynamic response to the cardiovascular changes associated with each trimester of pregnancy. First, a preliminary lumped parameter model of the non-pregnant woman circulation was developed, including the heart, the systemic circulation with a specific block for the uterine district and the pulmonary circulation. The model was first tested at rest; then heart rate and vascular resistances were individually varied to verify the correct response to parameter alterations characterising pregnancy. In order to simulate hemodynamics during pregnancy at each trimester, the main changes applied to the model consisted in reducing vascular resistances, and simultaneously increasing heart rate and ventricular wall volumes. Overall, reasonable agreement was found between model outputs and *in vivo* data, with the trends of the cardiac hemodynamic quantities suggesting correct response of the heart model throughout pregnancy. Results were reported for uterine hemodynamics, with flow tracings resembling typical Doppler velocity waveforms at each stage, including pulsatility indexes. Such a model may be used to explore the changes that happen during pregnancy in women with cardiovascular diseases.

Keywords

Lumped parameter model; uterine circulation; vasodilation; pregnancy-induced adaptations.

Graphical abstract

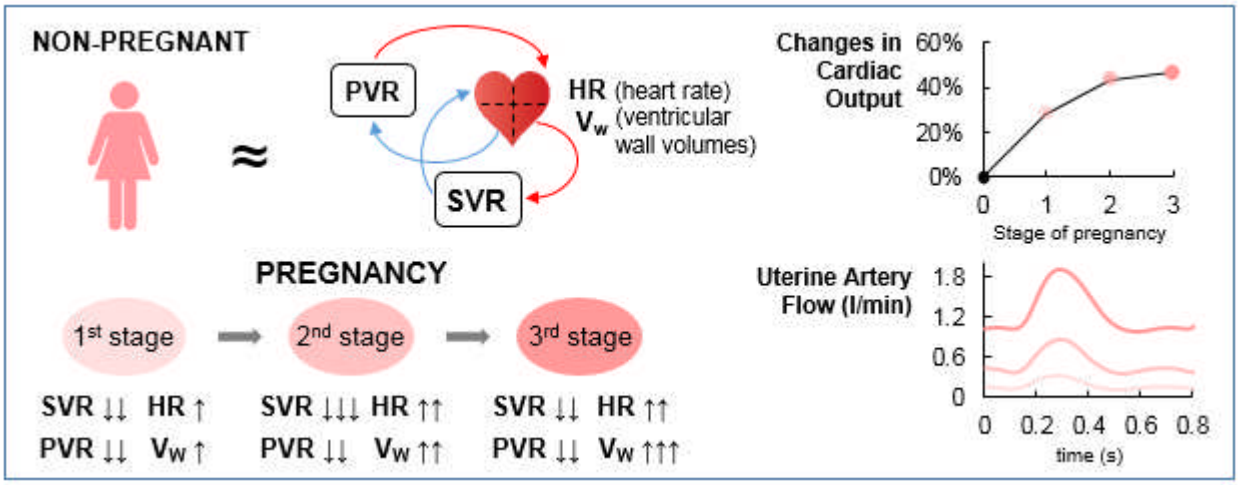

Abbreviations

CO – cardiac output

CVP – central venous pressure

EDV – end-diastolic volume

ESV – end-systolic volume

HR – heart rate

LB – lower body

LPM – lumped parameter model

LV – left ventricle

MAP – mean aortic pressure

PI – pulsatility index

PVR – pulmonary vascular resistance

RV – right ventricle

SV – stroke volume

SVR – systemic vascular resistance

UB – upper body

Introduction

Pregnancy is associated with physiologically significant but reversible changes in maternal hemodynamics and cardiac function in response to both foetal and maternal demands. Namely, maternal circulation needs to accommodate for an increase in blood volume to provide the nutrients and oxygen supply necessary for an optimal growth of the foetus through the placental circulatory system. In most women these demands are met without compromising the mother but they may prove to be a threat in mother with cardiovascular diseases. Conversely, if maternal hemodynamics do not change, adverse effects on the uteroplacental circulation can lead to foetal compromise. Therefore the maternal cardiovascular system must achieve a balance between foetal needs and maternal tolerance. Changes happen throughout the pregnancy: they begin as early as 4-5 weeks of gestation to facilitate the development of an optimal environment for the foetus to thrive, and tend to plateau during the second and early third trimesters [1]. Maternal adaptations differ according to the involved tissue or organ, and, due to the dynamic nature of pregnancy, the timing and degree of adaptation may vary between subjects. However, it is possible to distinguish common hemodynamic phenomena characterising each trimester of physiological pregnancies. Major changes include increase in blood volume, cardiac output, heart rate and oxygen consumption, decrease in systemic vascular resistance and alteration in distribution of blood flow favouring pregnant uterus, breasts and kidneys.

Systemic vascular resistance (SVR) decreases in early pregnancy, reaching the minimum in the second trimester (-30% to -35% compared to values observed 3 to 6 months after delivery), and subsequently rising up to -20÷-27% [2,3]. This is due to systemic vasodilatation mediated by hormonal changes and the opening of the low resistance uteroplacental circulation. Plasma volume and red blood cell mass progressively increase until the beginning of the third trimester, when they start stabilising until delivery [4]. Nevertheless, the larger increase in plasma volume with respect to the haematocrit is responsible for an approximately 10% decrease in total blood viscosity, facilitating diffusion across the placenta and avoiding thromboembolic risks for the mother. Besides haemodilution, peripheral arterial vasodilation is the main responsible for SVR reduction, which, in turn, activates compensatory homeostatic mechanisms allowing for the maintenance of arterial blood pressure. Namely, the heart rate (HR) increases from the first trimester, gradually reaching +20% in the third one. Similarly, the stroke volume (SV) rises in the first trimester to a maximum of around +30% in the second trimester without significant changes in the remaining weeks [5]. Consequently, the cardiac output (CO) begins to

increase at few weeks of gestation, continuing steadily and plateauing (around +40%) at 32 weeks [5]. While the rise in CO is mainly caused by the increase in SV during the early stages, HR contributes the most in late pregnancy when SV is nearly constant.

The vascular district showing the most significant flow increase is the uterine circulation, peaking at 10-20% of CO in the third trimester compared to about 1% in non-pregnant women [1,6]. Renal perfusion rises by more than 30% by mid-pregnancy, remaining constant until delivery. In addition, pulmonary blood flow rises throughout pregnancy, as a consequence of considerable reduction (about -30% at the end of the first stage and plateauing in the rest of gestation) in pulmonary vascular resistance (PVR) [7,8].

The physiological changes in preload and afterload of the heart, related to blood volume increase and peripheral vasodilation respectively, are accompanied by remodelling of all four cardiac chambers. Ventricles progressively increase in their diastolic dimension, while atria augment their average size, from the first trimester to the end of pregnancy. To sustain the increased workload, data suggest the two ventricles experience a rise in their wall thickness and mass with some debate on the entity [9–11]. Emerging MRI data indicate an increase reaching about +48% and +39% for the left ventricle (LV) and right ventricle (RV), respectively, at late pregnancy [12].

So far, plenty of clinical data has been collected for the analysis of such an intricate network of phenomena characterising pregnancy [2–5] and hypotheses on the physiological pathways have been advanced with no definitive answers. Most of the engineering studies has focused on the foetal circulation, especially on the placental gas exchange [13–17]. However, no mathematical models have been developed to examine the effects of pregnancy on the maternal cardiovascular system. The present study aims to develop a mathematical model of the pregnant woman circulation, in order to investigate the hemodynamic response of the model to the cardiovascular changes associated with each trimester of pregnancy, and compare it with literature data. A deeper understanding of the hemodynamic changes in healthy pregnancies is mandatory to get to a better understanding, and therefore better management strategies, of pregnancies in mothers with pre-existing cardiovascular diseases or arisen complications.

Materials and methods

Mathematical modelling of the circulatory system during pregnancy was achieved through several consecutive steps. First, a lumped parameter model (LPM) of the circulation of a healthy non-pregnant woman was developed, based on literature models of adult male

circulations [18,19]. This was accomplished by adding a block representing the uterine circulation, and scaling the lumped parameters according to proper powers of the body weights ratio [20], assuming 75 kg body weight for the male model and 58 kg as representative of a 30-year-old woman body weight. The LPM included the heart, the upper body (UB) and lower body (LB) systemic circulations, and the pulmonary circulation (Fig. 1, top). Systemic and pulmonary districts included great vessels and peripheral vasculatures, which were divided into arterial-arteriolar, capillary and venous portions. Three-element models comprising a compliance, a linear resistance and an inertance represented the great vessels and the arterial-arteriolar portions of peripheral vasculatures, whereas blocks including one or more compliances and resistances were used for the capillary and venous portions of peripheral vasculatures and for the abdominal organs circulations. Heart valves were described by three-element models comprising an inertance, a linear resistance and a non-linear resistance, combined with a diode assuring unidirectional flow (Fig. 1, bottom). The resting state was simulated at a HR of 75 beats per minute (bpm). Then, the model was tested at increasing HR and varying vascular resistances in order to verify the response to parameter changes involved in pregnancy. After these procedures, model parameters were modified according to the circulatory scenarios characterising the physiology of each gestational phase, and the resulting hemodynamic quantities were evaluated. The LPM was implemented in Matlab® R2014b (The MathWorks, Inc.) using, as integration algorithm, the Runge-Kutta-Fehlberg of the $4^{th}/5^{th}$ order with variable time step ranging from 1e-6 s to 1e-3 s. For each model configuration, 30 cardiac cycles were simulated to assure periodicity of the solution, but only the last 3 cycles were used for calculation of time averaged values. The entire simulations required less than 2 minutes on an Intel® Core™ i7 (2.93 GHz) personal computer.

Heart model

The heart model was based on the single fibre approach, which directly relates the macroscopic biomechanical behaviour of the ventricular chamber to the microscopic mechanical properties of myocardial sarcomere, i.e. the contractile element of cardiac tissue [21,22]. The choice of the heart model for this study was driven by the limited number of parameters required by the single fibre model and by the use of parameters representing physical quantities that could be either based on experimental observations or derived from clinical data. Blood pressure within the chamber was derived by stress and strain along the myocardial fibre direction and those along the radial wall direction. Assuming the healthy cardiac chamber as a thick-walled sphere, its mechanical behaviour was approximated by

a single fibre due to the homogeneous distribution of stress and strain within the tissue. In this setting, the cavity pressure P could be proportionally derived from the myocardial stress fusing anatomical data, i.e. the chamber volume V and the wall volume V_w, as follows:

$$P = \frac{\sigma_f + 2\sigma_{m.r}(\bar{r})}{1+3V/V_w} \quad (1)$$

where σ_f is the fibre stress and $\sigma_{m.r}(\bar{r})$ is the wall stress generated in the collagen matrix along the radial direction, at a representative radial position $\bar{r}$ enclosing the chamber volume and one third of the wall volume. This position was previously introduced by Bovendeerd and colleagues [22] to evaluate the integral of $\sigma_{m.r}$ over the wall thickness, since it is spatially inhomogeneous. They used the above described approach to model only the left ventricle (LV), while a similar description was extended to the right ventricle (RV) by Cox et al., owing to the similar microscopic tissue properties between the two chambers [23]. In the present study, this approach was implemented for the two atria as well, by applying scaling factors that will be described further on.

The total fibre stress σ_f is composed of an active stress (σ_a) and a passive stress component ($\sigma_{m.f}$) generated in the collagen matrix along the fibre direction. σ_a is defined by three terms: a function of the sarcomere length l_s, a time-varying term and a function of the sarcomere shortening velocity v_s, as follows:

$$\sigma_a(l_s, t, v_s) = c[f(l_s)A(t)h(v_s)] \quad (2)$$

with c being a coefficient ($0 \leq c \leq 1$) able to simulate a reduction in contractility for values approaching 0. The function $f(l_s)$ was based on that presented in [22] for the ascending tract of the curve, and inspired by the experimental findings obtained by Fabiato et al. [24] and Weiwad et al. [25] as regards the second tract of the curve (Fig. 2a). These studies detected a decrease in the force developed by skinned cardiac myocites for a sarcomere length over a threshold, $l_{s.max}$, and zero force at length = $l_{s.end}$. Being $f_{max} = f(l_{s.max})$, the definition of $f(l_s)$ is the following:

$$f(l_s) = \begin{cases} 0 & if\ l_s \leq l_{s.a0} \\ f_{ar}\left(\frac{l_s - l_{s.a0}}{l_{s.ar} - l_{s.a0}}\right) & if\ l_{s.a0} < l_s \leq l_{s.max} \\ f_{max}\left(\frac{l_s - l_{s.max}}{l_{s.max} - l_{s.end}} + 1\right) & if\ l_s > l_{s.max} \end{cases} \quad (3)$$

Time dependency was described by the periodic function $A(t)$ with period equal to the cardiac cycle, T_c, in two distinct ways for the ventricular ($AV(t)$) and atrial ($AA(t)$) chambers, respectively (Fig. 2b).

$$AV(t) = \begin{cases} \left[0.5\left[1 - \cos\left(\frac{2\pi t}{T_{vs}}\right)\right]\right]^{0.7} & if\ 0 \le t < T_{vs} \\ 0 & if\ T_{vs} \le t < T_c \end{cases} \quad (4)$$

$$AA(t) = \begin{cases} 0.5\left[1 - cos\left(\frac{2\pi(t+T_{as}-T_{ov})}{T_{as}}\right)\right] & if\ 0 \le t < T_{ov}\ \ or\ \ T_c - T_{as} + T_{ov} \le t < T_c \\ 0 & if\ \ T_{ov} \le t < T_c - T_{as} + T_{ov} \end{cases} \quad (5)$$

$T_{vs} = \alpha T_{QT}$ is the duration of ventricular systole and is defined as a fraction α of the duration of the QT wave indicating ventricular electrical activity on the electrocardiogram. Based on the relationship between T_{vs} and T_c proposed by Avanzolini et al. [26], and using the polynomial function reported in [18] to calculate T_{QT} from T_c, α resulted about 1.1 at any HR value. $T_{as} = \beta T_{vs}$ is the duration of atrial systole while $T_{ov} = \gamma T_{as} - 0.05$ is the overlap interval between $AV(t)$ and $AA(t)$.

The third term in Equation 2, $h(v_s)$, represents the viscous contribution of the fibre to the total active stress [22].

The passive stress along the fibre direction $\sigma_{m.f}$ and along the radial direction $\sigma_{m.r}$ were defined as functions of the fibre stretch ratio λ_f and the radial stretch ratio λ_r, respectively [22]. Considering the passive chamber at zero transmural pressure with volume V_0 (corresponding to a sarcomere length l_{s0}) as the reference state, λ_f and λ_r could be approximated by volumetric ratios, as follows:

$$\lambda_f = \frac{l_s}{l_{s0}} \approx \left(\frac{V + 1/3V_w}{V_0 + 1/3V_w}\right)^{1/3} \quad \text{and} \quad \lambda_r = \left(\lambda_f\right)^{-2} \quad (6)$$

It is worth noting that, with such notation, λ_f represents the circumferential stretch ratio at the above mentioned radial position $\bar{r}$ [22]. All the parameters used in Equations 2-6 are reported in Table 1 and Table 2. Additionally, scaling factors were applied to the active and passive stresses of the two atria in order to account for the different tissue contents of the atrial walls compared with those in the ventricular walls. Based on the percentages of muscle fibres and extra-cellular matrix of the atrial walls provided in [27] active and passive scaling

factors were derived, respectively, as ratios over the corresponding percentages of the LV wall, which is the heart chamber used as a reference for developing the single fibre approach. Values of 0.84 and 1.17 were utilised as the active and passive scaling factors, respectively, for the left atrium, whereas 0.81 and 1.19 for the right atrium.

The chamber wall volumes used in this study (Tab. 2) were consistent with data collected from the literature [10,27–30]. Since reference volumes V_0 are not measurable *in vivo*, their values were tuned starting from the end-systolic (i.e. minimum) volumes (ESV) reported in the literature, in order to obtain pressure-volume loops consistent with the physiological range for a healthy woman [30,31].

Systemic and pulmonary circulations models

As per conventional clinical practice, the global vascular resistances of the model were calculated using the following formulas:

$$SVR = \frac{\overline{P_{AO}} - \overline{P_{RA}}}{\overline{Q_s}} \qquad PVR = \frac{\overline{P_{PA}} - \overline{P_{LA}}}{\overline{Q_p}} \tag{7}$$

where $\overline{P_{AO}}$, $\overline{P_{RA}}$, $\overline{P_{PA}}$ and $\overline{P_{LA}}$ are the time-averaged pressures in the aorta, right atrium, pulmonary arteries and left atrium, respectively, whereas $\overline{Q_s}$ and $\overline{Q_p}$ are the time-averaged flow rates in the systemic and pulmonary circulations, respectively (note that in a healthy subject $\overline{Q_s} = \overline{Q_p} = CO$ i.e. the cardiac output). From the scaling procedure, the SVR and PVR resulted 17.4 WU and 1.63 WU, respectively (1 WU or Wood Unit = 1 mmHg/L*min = 7.99 MPa/m^3*s), in agreement with data reported in the literature [7,10]. The model layout was detailed to allow implementation of the hemodynamic changes due to pregnancy (Fig. 1). Namely, the UB was divided between brain and arms, while the LB great vessels were subdivided into thoracic and abdominal portions to accommodate the abdominal organs, including the uterine circulation. The latter was based on a previously developed model of the uterine circulation in the third trimester [32], using the same percentage resistance distribution but scaling resistance values in order to have a uterine flow lower than 1% of CO [6]. Uterine compliance values were scaled as well, according to the relationship between compliances and resistances described in [19].

Fine tuning of the systemic circulatory parameters was performed in order to reach a 30:70 CO distribution to the UB and LB vasculatures [33], as well as a proper splitting among the

individual vascular districts and a mean aortic pressure (MAP) at rest of approximately 80 mmHg.

Models of the three stages of pregnancy

In order to simulate maternal hemodynamics during pregnancy, clinical data were collected from the literature for each trimester as percentage variations from the reference state i.e. non-pregnant condition at rest [3,7–12,28]. It is worth noting that most of the studies considered the state at 3-to-6 months after delivery as the reference, since it is a reasonable span for hemodynamics to return to baseline, and that the ranges of variations within each investigated population might partly disagree between studies due to the different ages or different positions during measurement acquisition. Moreover, extensive data were not available for all the vascular districts e.g. the right ventricle, the atria, peripheral resistances and compliances other than those of the uterine vasculature, as well as for all trimesters (i.e. the first two stages have been less investigated so far compared to the third). In order to implement relevant information from collected data inside our model i.e. apply changes to global parameters, we either calculated average values, when available, or assumed them as reported in Table 3. Based on ventricular wall volumes in the non-pregnant condition, changes in LV V_w in all trimesters and RV V_w only in the third one, RV V_w values for the first and second stage were derived by assuming the ratio over LV V_w as approximately constant (≈ 0.2).

Reductions of SVR were unevenly applied to the vascular districts in order to account for the unbalance in the flow rate distribution caused by the development of uteroplacental circulation and by selective vasodilation characterising pregnancy. Based on the information about the trends followed by flow distribution throughout systemic circulation and by cardiac volumes during each trimester [3,10–12,34–38], resistances of the uterine, renal, cerebral and intestinal districts were decreased accordingly, whereas volumes V_0 of the four heart chambers were increased by assumed percentages (Tab. 4). In addition, resistances of the remaining systemic districts were decreased by the same percentage with respect to the non-pregnant values (Tab. 4) in order to obtain the desired reductions in SVR (Tab. 3). Such changes were consistent with blood viscosity reduction and, for the first and second trimesters, might be ascribed to further vasodilatory effects. Within the individual systemic districts as well as in the pulmonary blocks, changes were evenly applied to the resistances

(i.e. arterial-arteriolar, capillary and venous), assuming that resistance ratios do not vary during pregnancy. The little information about changes in vascular distensibility found in the literature regarded the reduction in arterial stiffness and increase in venous tone, which both facilitate cardiac function by decreasing afterload on the one hand, and augmenting preload on the other. This allowed us to directly increase compliances of the aorta and major systemic arteries by +18%, +14% and +25%, while reducing venous compliances of the legs by -20%, -25% and -30% in the first, second and third trimester, respectively [28,35]. However, for the other districts, the applied decreases in resistances were followed by corresponding growths in compliances and decreases in inertances [19].

Results

Non-pregnant model

The model of the adult female circulation in the non-pregnant condition at rest showed mean values of hemodynamic quantities within the ranges reported in the literature (Tab. 5). Flow distribution throughout systemic circulation was also in agreement with available *in vivo* data (Tab. 5). In particular, the time-averaged uterine flow rate was 0.35 ml/s, with a pulsatility index (PI) of 1.63 being in the range of typical values observed in non-pregnant healthy women [6,39].

Ventricular volumes and pressures reflected those reported for healthy subjects [9,12,29,30]: RV ESV and end-diastolic volumes (EDV) were higher than the respective LV values, resulting in the same SV (≈ 65 ml), while RV pressures were considerably lower (≈ 1/4) than LV pressures (Fig. 3).

The model response to individual changes in SVR and PVR in terms of CO revealed roughly linear behaviours with a greater influence of the former compared to the latter for equal changes in resistances: 200% increase in either SVR or PVR resulted in CO reductions of about -50 % and -20%, respectively (Fig. 4, *left*). The trend exhibited by CO with increasing HR showed a plateau between 180 bpm and 220 bpm, followed by a significant drop (Fig. 4, *right*). Conversely, SV showed a monotonic decrease with HR as depicted in Figure 4 (*right*).

Models of the three stages of pregnancy

The model response to the hemodynamic modifications introduced to simulate pregnancy was evaluated for each trimester as percentage variation from the non-pregnant condition. Figure 5 shows the trends depicted by CO and SV along the three gestational stages. CO

increased significantly from the first (+28%) throughout the second trimester (+44%), nearly reaching a plateau at the end of gestation (+46%). The SV behaviour reflected the CO trend in the first two trimesters (+16% and +25%, respectively), but increased to lower extent in the third phase (+22%). These trends were in agreement with *in vivo* data collected from the literature [9–11,28,40], as illustrated by figure 5.

Increases in the pulmonary and systemic flows were analogous to those of CO, with greater percentages related to the LB flow (+32%, +49% and +55% for the first, second and third trimester, respectively) compared to the UB flow (+18%, +29% and +22%). Pregnancy augmented flow rates perfusing all local vasculatures throughout all trimesters, except for flow in the legs, which reported slight increases (≤+10%) in the first two stages and a minor decrease (>-3%) in the last stage. Uterine flow experienced the highest increase during the entire course of pregnancy, reaching 3%, 8% and 18% of CO in the first, second and third trimester, respectively. PI values were reduced to 1.13, 1.09 and 0.72 gradually at each trimester, as displayed by the time tracings of uterine artery flow (Fig. 6). Among the other vascular districts, kidneys showed the highest rise in flow, peaking at +80% in the first trimester and progressively decreasing to +50% in the third trimester.

Both ventricle EDV did not vary considerably in the first trimester (<1% as absolute values), and increased in the last two up to +19% and +22% for LV and RV, respectively. The ESV values, instead, decreased in the first stage by -20% and -16% for LV and RV, respectively; afterwards they began rising up to +14% and +21% in the last stage. As a consequence, the trends of ventricular ejection fractions were described by an initial growth (+17%) which gradually dropped to non-pregnant values. Maximum atrial volumes increased from the first trimester up to +22% and +32% for the left and right atrium, respectively, in the last trimester. Finally, pressures were moderately stable, with changes lower than 10% (as absolute values) in the systemic circulation and 4% in the pulmonary vasculature (Tab. 6). Larger variations occurred in the central venous pressure (CVP), which increased to 5.8 mmHg in the first trimester and diminished to 4.1 mmHg in the last stage (Tab. 6).

Discussion

Pregnancy is characterised by several physiologic adaptations of the mother's body in response to both foetal and maternal demands, possibly starting with peripheral vasodilation of systemic and pulmonary districts mediated by hormones and vasoactive molecules, and subsequently followed by observed increases in plasma volume, CO, HR and ventricular mass. Such mechanisms allow the mother to maintain adequate systemic and pulmonary

blood pressures ultimately to guarantee the correct regional perfusion including the newly developed uteroplacental circulation that supplies the growing foetus. These changes have been clinically described extensively but a complete and thorough understanding of the complex pathways involved (i.e. endocrine, autonomic, cytokines mediated) is still lacking. Moreover, despite the availability of clinical data, mathematical models have not been developed so far to include all these data in a consistent theoretical framework that allows one to examine the influence of pregnancy on maternal hemodynamics. This study presents a mathematical model of the pregnant woman circulation to evaluate its response to the cardiovascular changes associated with each gestational stage.

An LPM of the non-pregnant woman circulation was developed as preliminary condition. First, the model was tested at rest (i.e. HR = 75 bpm), then by individually varying HR, SVR and PVR. Mean values of pressures, flows and ventricular volumes resulted in agreement with *in vivo* data (Tab. 5) [2,6,7,9,11,29,33]. In particular, the uterine flow exhibited time-average and PI values typical of non-pregnant women [6,39]. As expected, the influence of SVR on CO was proportionally greater than that exerted by PVR (Fig. 4, *left*), due to the ratio of about 10:1 between the two vascular resistances. Progressively increasing HR led to an initial increase in CO, followed by a plateau and a further drop (Fig. 4, *right*). In fact, CO depends not only on HR but also on SV, which conversely exhibited a monotonic decrease with HR (Fig. 4, *right*), as observed *in vivo* under electrical stimulation of the right atrium [41].

Appropriate changes to HR, cardiac volumes V_w and V_0, and LPM parameters (i.e. resistances, compliances and inertances) were introduced to simulate pregnancy, and the model response was evaluated as percentage variation from the non-pregnant condition. The trends followed by CO and SV throughout the simulated gestation were in agreement with *in vivo* data from literature [9,10,28], especially with the narrow ranges observed in the third trimester for both quantities [9,11,36,40] (Fig. 5). The lesser increase in SV in the third trimester (+22%) compared to the second trimester (+25%) reflected *in vivo* observations of the aortocaval compression exerted by the enlarged uterus [9]. Such phenomenon was taken into account in our model by imposing higher SVR in the third stage with respect to the previous one. As regards ventricular volumes, the resulting gradual increase in LV EDV replicated the trends reported by Katz *et al.* [34] and by Cong *et al.* [11]. Similarly, the RV EDV obtained for the third trimester was highly close to the only reference found for the RV (+22% vs. +24%) [12]. Contrary to the measurements performed by Cong and colleagues [11], the LV ESV diminished in the first trimester. In our model, this was due to an increase

in ventricular mass not accompanied by an immediate rise in EDV (nearly null), which instead was reported as +7% by the same authors. Consequently, the LV ejection fraction initially increased by 17% to reach non-pregnant values only at the end of gestation, whereas changes observed by Cong *et al.* did not exceed 3% during the whole pregnancy [11]. An extensive comparison with *in vivo* data was not possible for the atrial volumes, due to the lack of information from the literature. Nevertheless, two recent clinical studies reported similar growths of the maximum atrial volumes in the second and third trimesters [12,42]. Globally, cardiac hemodynamics results suggested a proper response of the heart model when applying known changes in HR and ventricular V_w (Tab. 3) and assumed values for ventricular and atrial V_0 (Tab. 4) for each stage.

Concerning the flow distribution, higher increases involved the LB compared to the UB circulation through all stages, owing to the considerable rise in perfusion of the uteroplacental and renal districts, as well as of the intestine in the last two stages. Such behaviour was achieved by properly varying the impedances of the relative vasculatures. Major results were reported by uterine hemodynamics, being overall in agreement with *in vivo* data [43,44]. The massive increase in uterine blood flow obtained with the model contributed to a “steal” phenomenon to the detriment of flow in the legs, as observed in the external iliac artery by Palmer and colleagues [45]. The average uterine artery flow obtained for the third trimester (1.29 l/min) exceeded the range observed in the literature (0.75-0.97 l/min) [44], as the flow value used for setting the uterine resistance in this trimester was measured from the uteroplacental circulation i.e. including the ovarian artery. The time tracings depicted by uterine artery flow (Fig. 6) resembled typical Doppler velocity waveforms in the uterine artery in the three gestational stages [46,47], with progressive decrease in pulsatility and disappearance of the diastolic notch. This was confirmed by PI values which were comparable with those reported by Tayyar *et al.* i.e. 1.6, 1.05 and 0.75 in the first, second and third trimester, respectively [48], thus revealing proper setting of the model parameters.

The trends followed by pressures (Tab. 6) generally reflected the literature data. In the second and third trimesters, MAP presented slightly higher values compared with the clinical counterpart (-5.3% and +9.3% vs. -13%÷-9% and -7%÷+4.5%, respectively) [3,7,34,49]. It is worth noting, however, that clinical ranges indicate high variability in such a quantity which may be ascribed to the different ages of the patients or positions (i.e. supine or left lateral recumbent) during measurement. Finally, CVP showed mild fluctuations around the non-pregnant value throughout gestation, first increasing by +25% and then decreasing to a

lower value (-12%). The few literature data collected for CVP during pregnancy seem in contrast with our results and between them: in one study significant changes were not registered at the third trimester [7], whereas, in another study, CVP in women in the last gestational phase was found to be much lower than that of non-pregnant or first-half pregnant women [50]. This might be due to the fact that pressure was measured in supine position causing compression of the inferior vena cava from the gravid uterus, thus reducing venous return and CVP.

Limitations of the presented model were mainly due to the fact that changes affecting metabolism or body systems other than maternal circulation (e.g. lymphatic system, foetal circulation and exchange with maternal side) during pregnancy were neglected. Therefore, comparison of our results, deriving from mere hemodynamic effects, with clinical measurements might be undermined by such model defaults. Moreover, collected literature data themselves were sometimes lacking or discordant, impairing any possible elaborate discussion. In order to create a more accurate model of maternal physiology, it would be recommendable to implement the complex network of maternal and foetal systems, as well as to collect a full dataset from a sufficiently large cohort of healthy pregnant patients recruited before conception (i.e. reference condition) although ethical issues regarding studying healthy pregnancies limit the type of tests, and screening before conception makes recruitment more difficult. Nevertheless, this was not the scope of the study, since the present mathematical model was developed as a preliminary effort to merge clinical data into a framework enabling a consistent analysis of the influence of pregnancy on maternal hemodynamics. A better understanding of hemodynamics in normal pregnancies through modelling is crucial and will give us a more solid background when looking at how acquired or congenital cardiovascular diseases impact on outcome for both mother and baby in more complex pregnancy settings. For example, the effects of maternal hypertension, known as pre-eclampsia, on the foetal circulation may be suitably investigated using a sophisticated version of the LPM presented in this study. Although the exact causes of pre-eclampsia are unknown, it seems it is related to impaired placental growth and perfusion [51] which might be implemented in the model as an overall increased placental impedance. Another interesting issue to consider would be the presence of congenital heart diseases such as cyanotic defects in the mother, which remarkably affect blood and oxygen supply to the foetus. The circulatory layout of the current model may be appropriately modified to examine the influence of such complex pregnancy conditions, by focusing on the heart and integrating with a model of the oxygen exchange between maternal and foetal circulations. However, in

both cases the availability of thorough clinical datasets would be essential to build models which can accurately describe these phenomena.

Conclusion

In this study a mathematical model of the healthy pregnant woman circulation was developed to investigate the hemodynamic response to the cardiovascular changes associated with each gestational stage. Results were compared with clinical measurements taken from the literature to assess the goodness of the model in terms of variations of hemodynamic quantities with respect to the non-pregnant condition. Overall, reasonable agreement was found between model outputs and *in vivo* data, suggesting a good description of maternal physiology. In addition to simulating healthy pregnancy, such a model may have great potential to explore the abnormal changes associated to pre-existing maternal diseases (e.g. congenital heart defects) or concurrent cardiovascular complications (e.g. pre-eclampsia) affecting pregnant hemodynamics.

Acknowledgements

The study was partially supported by Fondation Leducq, Paris, through the Trans-Atlantic Network of Excellence for Cardiovascular Research grant ‘Multi-Scale Modelling of Single Ventricle Hearts for Clinical Decision Support’. The authors would like to acknowledge Anna Gargantini (M.Eng.) and Simona Scalabrino (M.Eng.) for their contribution in developing the model.

References

[1] Blackburn ST. Maternal, fetal, & neonatal physiology: a clinical perspective. 4th ed. Elsevier Saunders; 2013.

[2] Bridges EJ, Womble S, Wallace M, Mccartney J. Hemodynamic monitoring in high-risk obstetrics patients, I. Expected hemodynamic changes in pregnancy. Crit Care Nurse 2003;23:53–62.

[3] Chapman AB, Abraham WT, Zamudio S, Coffin C, Merouani A, Young D, et al. Temporal relationships between hormonal and hemodynamic changes in early human pregnancy. Kidney Int 1998;54:2056–63.

[4] Norwitz ER, Robinson JN. Pregnancy-induced physiologic alterations. In: Belfort MA, Saade G, Foley MR, Phelan JP, Dildy GA, editors. Crit. Care Obstet., Chichester: Wiley-Blackwell; 2010, p. 30–52.

[5] Silversides CK, Colman JM. Physiological changes in pregnancy. In: Oakley C, Warnes CA, editors. Hear. Dis. pregnancy, Malden: Blackwell Publishing; 2007, p. 6–17.

[6] Hale SA, Schonberg A, Badger GJ, Bernstein IM. Relationship between prepregnancy and early pregnancy uterine blood flow and resistance index 2009;16:1091–6.

[7] Clark SL, Cotton DB, Lee W, Bishop C, Hill T, Southwick J, et al. Central hemodynamic assessment of normal term pregnancy 1989;161:1439–42.

[8] Robson SC, Hunter S, Boys RJ, Dunlop W. Serial changes in pulmonary hemodynamics during pregnancy: a non-invasive study using Doppler echocardiography. Clin Sci 1991;80:113–7.

[9] Robson SC, Hunter S, Boys RJ, Dunlop W. Serial study of factors influencing changes in cardiac output during human pregnancy. Am J Physiol Hear Circ Physiol 1989;256:H1060–H1065.

[10] Geva T, Mauer MB, Striker L, Kirshon B, Pivarnik JM. Effects of physiologic load of pregnancy on left ventricular contractility and remodeling. Am Heart J 1997;133:53–9.

[11] Cong J, Fan T, Yang X, Squires JW, Cheng G, Zhang L, et al. Structural and functional changes in maternal left ventricle during pregnancy: a three-dimensional speckle-tracking echocardiography study. Cardiovasc Ultrasound 2015;13:6.

[12] Ducas RA, Elliott JE, Melnyk SF, Premecz S, DaSilva M, Cleverley K, et al. Cardiovascular magnetic resonance in pregnancy: insights from the cardiac hemodynamic imaging and remodeling in pregnancy (CHIRP) study. J Cardiovasc Magn Reson 2014;16:1.

[13] Luria O, Bar J, Kovo M, Golan A, Barnea O. Feto-maternal interaction: a mathematical model simulating placental response in hypertensive disorders of pregnancy. Reprod Sci 2010;17:963–9.

[14] van den Wijngaard JP, Westerhof BE, Faber DJ, Ramsay MM, Westerhof N, van Gemert MJ. Abnormal arterial flows by a distributed model of the fetal circulation. Am J Physiol Regul Integr Comp Physiol 2006;291:R1222-33.

[15] Yigit MB, Kowalski WJ, Hutchon DJR, Pekkan K. Transition from fetal to neonatal circulation: modeling the effect of umbilical cord clamping. J Biomech 2015;48:1662–70.

[16] Pennati G, Corno C, Costantino ML, Bellotti M. Umbilical flow distribution to the liver and the ductus venosus in human fetuses during gestation: an anatomy-based mathematical modeling. Med Eng Phys 2003;25:229–38.

[17] Pennati G, Bellotti M, Fumero R. Mathematical modelling of the human foetal cardiovascular system based on Doppler ultrasound data. Med Eng Phys 1997;19:327–35.

[18] Liang F, Senzaki H, Kurishima C, Sughimoto K, Inuzuka R, Liu H. Hemodynamic performance of the Fontan circulation compared with a normal biventricular circulation: a computational model study. Am J Physiol Heart Circ Physiol 2014;307:H1056-72.

[19] Kung E, Pennati G, Migliavacca F, Hsia T-Y, Figliola R, Marsden A, et al. A simulation protocol for exercise physiology in Fontan patients using a closed loop lumped-parameter model. J Biomech Eng 2014;136:1–13.

[20] Pennati G, Fumero R. Scaling approach to study the changes through the gestation of human fetal cardiac and circulatory behaviors. Ann Biomed Eng 2000;28:442–52.

[21] Arts T, Bovendeerd P, Delhaas T, Prinzen F. Modeling the relation between cardiac pump function and myofiber mechanics. J Biomech 2003;36:731–6.

[22] Bovendeerd PHM, Borsje P, Arts T, Van De Vosse FN. Dependence of intramyocardial pressure and coronary flow on ventricular loading and contractility: a model study. Ann Biomed Eng 2006;34:1833–45.

[23] Cox LGE, Loerakker S, Rutten MCM, de Mol BAJM, van de Vosse FN. A mathematical model to evaluate control strategies for mechanical circulatory support. Artif Organs 2009;33:593–603.

[24] Fabiato A, Fabiato F. Myofilament-generated tension oscillations during partial calcium activation and activation dependence of the sarcomere length-tension relation of skinned cardiac cells. J Gen Physiol 1978;72:667–99.

[25] Weiwad WK, Linke W a, Wussling MH. Sarcomere length-tension relationship of rat cardiac myocytes at lengths greater than optimum. J Mol Cell Cardiol 2000;32:247–59.

[26] Avanzolini G, Barbini P, Cappello A, Cevenini G. CADCS simulation of the closed-loop cardiovascular system. Int J Biomed Comput 1988;22:39–49.

[27] Arts T, Lumens J, Kroon W, Delhaas T. Control of whole heart geometry by intramyocardial mechano-feedback: A model study. PLoS Comput Biol 2012;8.

[28] Poppas A, Shroff SG, Korcarz CE, Hibbard JU, Berger DS, Lindheimer MD, et al. Serial assessment of the cardiovascular system in normal pregnancy. Role of arterial compliance and pulsatile arterial load. Circulation 1997;95:2407–15.

[29] Cain PA, Ahl R, Hedstrom E, Ugander M, Allansdotter-Johnsson A, Friberg P, et al. Age and gender specific normal values of left ventricular mass, volume and function for gradient echo magnetic resonance imaging: a cross sectional study. BMC Med Imaging 2009;9:2.

[30] Hudsmith L, Petersen S, Francis J, Robson M, Neubauer S. Normal human left and right ventricular and left atrial dimensions using steady state free precession magnetic resonance imaging. J Cardiovasc Magn Reson 2005;7:775–82.

[31] Maceira AM, Cosín-sales J, Roughton M, Prasad SK, Pennell DJ. Reference right atrial dimensions and volume estimation by steady state free precession cardiovascular magnetic resonance. J Cardiovasc Magn Reson 2013;15:1–10.

[32] Talbert DG. Uterine flow velocity waveform shape as an indicator of maternal and placental development failure mechanisms: a model-based synthesizing approach. Ultrasound Obstet Gynecol 1995;6:261–71.

[33] Kam P, Power I. Principles of physiology for the anaesthetist. 3rd ed. Boca Raton (FL): CRC Press; 2015.

[34] Katz R, Karliner J, Resnik R. Effects of a natural volume overload state (pregnancy)

on left ventricular performance in normal human subjects. Circulation 1978;58:434–441.

[35] Edouard D a, Pannier BM, London GM, Cuche JL, Safar ME. Venous and arterial behavior during normal pregnancy. Am J Physiol 1998;274:H1605-12.

[36] Clapp JF, Stepanchak W, Tomaselli J, Kortan M, Faneslow S. Portal vein blood flow - effects of pregnancy, gravity, and exercise. Am J Obstet Gynecol 2000;183:167–72.

[37] Dunlop W. Renal physiology in pregnancy. Postgrad Med J 1979;55:329–32.

[38] Nevo O, Soustiel JF, Thaler I. Maternal cerebral blood flow during normal pregnancy: a cross-sectional study. Am J Obstet Gynecol 2010;203:475.e1-475.e6.

[39] Zebitay AG, Tutumlu M, Verit FF, Ilhan GK, Gungor ES, Cetin O, et al. A comparative analysis of arterial blood flow in unexplained infertility, tubal infertility and fertile groups. Gynecol Endocrinol 2016;32:442–5.

[40] Pandey AK, Das A, Srinivas C, Babu MS, Himabindu Y, Kumar A, et al. Maternal myocardial performance in various stages of pregnancy and post-partum. Res J Cardiol 2010;3:9–16.

[41] Ross J, Linhart JW, Brauwald E. Effects of changing heart rate in man by electrical stimulation of the right atrium. studies at rest, during exercise, and with isoproterenol. Circulation 1965;32:549–58.

[42] Ando T, Kaur R, Holmes AA, Brusati A, Fujikura K, Taub CC. Physiological adaptation of the left ventricle during the second and third trimesters of a healthy pregnancy: a speckle tracking echocardiography study. Am J Cardiovasc Dis 2015;5:119–26.

[43] Browne VA, Julian CG, Toledo-Jaldin L, Cioffi-Ragan D, Vargas E, Moore LG. Uterine artery blood flow, fetal hypoxia and fetal growth. Philos Trans R Soc 2015;370:1–15.

[44] Konje JC, Kaufmann P, Bell SC, Taylor DJ. A longitudinal study of quantitative uterine blood flow with the use of color power angiography in appropriate for gestational age pregnancies. Am J Obstet Gynecol 2001;185:608–13.

[45] Palmer S, Zamudio S, Coffin C, Parker S, Stamm E, Moore L. Quantitative estimation of human uterine artery blood flow and pelvic blood flow redistribution in pregnancy. Obstet Gynecol 1992;80:1000–6.

[46] Miller J, Harman C. Comprehensive first-trimester prenatal assessment. Neoreviews 2009;10:e538–49.

[47] Gómez O, Figueras F, Fernández S, Bennasar M, Martínez JM, Puerto B, et al. Reference ranges for uterine artery mean pulsatility index at 11-41 weeks of gestation. Ultrasound Obstet Gynecol 2008;32:128–32.

[48] Tayyar A, Guerra L, Wright A, Wright D, Nicolaides KH. Uterine artery pulsatility index in the three trimesters of pregnancy: effects of maternal characteristics and medical history. Ultrasound Obstet Gynecol 2015;45:689–97.

[49] Estensen ME, Beitnes JO, Grindheim G, Aaberge L, Smiseth O a, Henriksen T, et al. Altered maternal left ventricular contractility and function during normal

pregnancy. Ultrasound Obstet Gynecol 2013;41:659–66.

[50] Colditz RiB, Josey WE. Central venous pressure in supine position during normal pregnancy: comparative determinations during first, second and third trimesters. Obstet Gynecol 1970;36:769–72.

[51] Oyston C, Baker PN. Therapeutic strategies for the prevention and treatment of pre-eclampsia and intrauterine growth restriction. Obstet Gynaecol Reprod Med 2017;23:375–80.

Table 1

Parameters of the sarcomere

Length (μm)					Stress (kPa)	Coefficients (-)		
l_{s0}	$l_{s.a0}$	$l_{s.ar}$	$l_{s.max}$	$l_{s.end}$	f_{ar}	c	β	γ
1.83	1.5	2.0	2.3	2.7	55	1	0.7	0.5

Table 2

Volumes of the heart chambers

(ml)	LV	RV	LA	RA
V_w	125	25	13.6	3
V_0	50	63	20	30

LV = left ventricle; RV = right ventricle; LA = left atrium; RA = right atrium.

Table 3

Reference state parameters and changes applied to the model for each trimester of pregnancy

	Non-pregnant	1st trimester	2nd trimester	3rd trimester
HR (bpm)	75	+10%	+15%	+20%
SVR (WU)	17.4	-30%	-35%	-27%
PVR (WU)	1.63	-30%	-30%	-30%
LV V_w (ml)	125	+10%	+31%	+45%
RV V_w (ml)	25	+6.6%*	+25%*	+30%

HR: heart rate; SVR/PVR: systemic/pulmonary vascular resistance; LV/RV V_w: left/right ventricle wall volume; bpm = beats per minute; 1WU = 1 mmHg/L*min = 7.99 MPa/m3*s. Changes were taken from the literature [2,3,8–12,28,49] and reported as percentages of the non-pregnant state parameters. Values with * were extrapolated from other clinical data.

Table 4

Parameter changes from the non-pregnant state applied to the model for each trimester of pregnancy

	1st trimester	2nd trimester	3rd trimester
Uterine resistance	-90%	-96%	-98%
Brain resistance	-10%	-17%	-8%
Renal resistance	-50%	-45%	-30%
Intestinal resistance			
- arterial	-24%	-45%	-30%
- venous	-24%	-35%	-20%
Liver resistance	-24%	-26%	-6%
Legs resistance	-24%	-26%	-6%
Arms resistance	-24%	-26%	-6%
Great vessels resistance	-24%	-26%	-6%
LV V_0	0%	+15%	+20%
RV V_0	0%	+20%	+30%
LA V_0	0%	+20%	+20%
RA V_0	0%	+30%	+30%

LV/RV and LA/RA V_0: left/right ventricle and left/right atrium volumes at zero transmural pressure.

Table 5

Results of the non-pregnant model at rest

	Results	Reference ranges
Systolic blood pressure (SBP)	114.9	104.2±10.7 [11] 123±11 [29]
Diastolic blood pressure (DBP)	68.1	64.4±8.0 [11] 72±8 [29]
Mean aortic pressure (MAP)	83.7	79.3±8.5 [11] 86.4±7.5 [7]
Central venous pressure	4.7	3.7±2.6 [7] 2÷6 [2]
Mean pulmonary artery pressure	19.9	15÷25 (S) [2] 8÷12 (ED) [2]
Cardiac output (CO)	4.8	4.3±0.9 [7] 4.9 [9]
Cerebral flow (%CO)	11.4%	12.9% [33]
Uterine flow (%CO)	0.44%	<1% [6]
Renal flow (%CO)	17.4%	19.0% [33]
Intestinal and hepatic flow (%CO)	21.4%	24.1% (AO) [33]

Pressures are in (mmHg); CO is in (l/min). Mean aortic pressure is calculated as done in clinical practice (i.e. SBP/3 + DBP*2/3). S: systolic; ED: end-diastolic; AO: abdominal organs excluding kidneys.

Table 6

Pressure results of the three stages of pregnancy as % variations from the non-pregnant condition

Pressures (mmHg)	Non-pregnant	1st trimester	2nd trimester	3rd trimester
Mean aortic pressure	83.7	-8.3%	-5.3%	+9.3%
Mean pulmonary artery pressure	19.9	-1.4%	-4.0%	-1.4%
Central venous pressure	4.7	+25%	+14%	-12%

Figure captions

Fig. 1 Schematic of the model. Colour-coded lumped parameter blocks are reported at the bottom. IVC: inferior vena cava; TH: thoracic; AB: abdominal. For the other acronyms, please refer to the list of abbreviations.

Fig. 2 Myocardial fibre stress. *Left:* active component $f(l_s)$ and passive stress $\sigma_{m.f}$ as functions of the sarcomere length l_s; $f(l_s)$ is periodically modulated in time by $AA(t)$, for the atria, and $AV(t)$, for the ventricles (*right*). Time modulation is indicated by the arrows. T_{ov}: overlap interval between $AV(t)$ and $AA(t)$; T_c: duration of cardiac cycle (i.e. period of $AV(t)$ and $AA(t)$); T_{vs}: duration of ventricular systole; T_{as}: duration of atrial systole.

Fig. 3 Pressure-volume loops of the left ventricle (LV) and right ventricle (RV).

Fig. 4 Non-pregnant model response to individual changes in model parameters: (*left*) cardiac output trends with varying systemic (SVR) and pulmonary (PVR) vascular resistances; (*right*) cardiac output (CO) and stroke volume (SV) trends with varying heart rate. SVR and PVR are reported as fractions of the respective values used in the non-pregnant model (i.e. unity on the x-axis).

Fig. 5 Cardiac output (*left*) and stroke volume (*right*) at each trimester. The model results are represented with black circles connected by a line, while *in vivo* data are displayed with different grey symbols according to the corresponding references. Adjacent symbols refer to the same values. ■ [9]; ▲ [3]; ● [28]; x [34]; ∗ [10]; ○ [11]; Δ [49].

Fig. 6 Uterine artery flow in the first, second and third trimesters. *Right*: close-up of the first trimester flow shows the marked pulsatility and the diastolic notch (arrow).

Figure 1

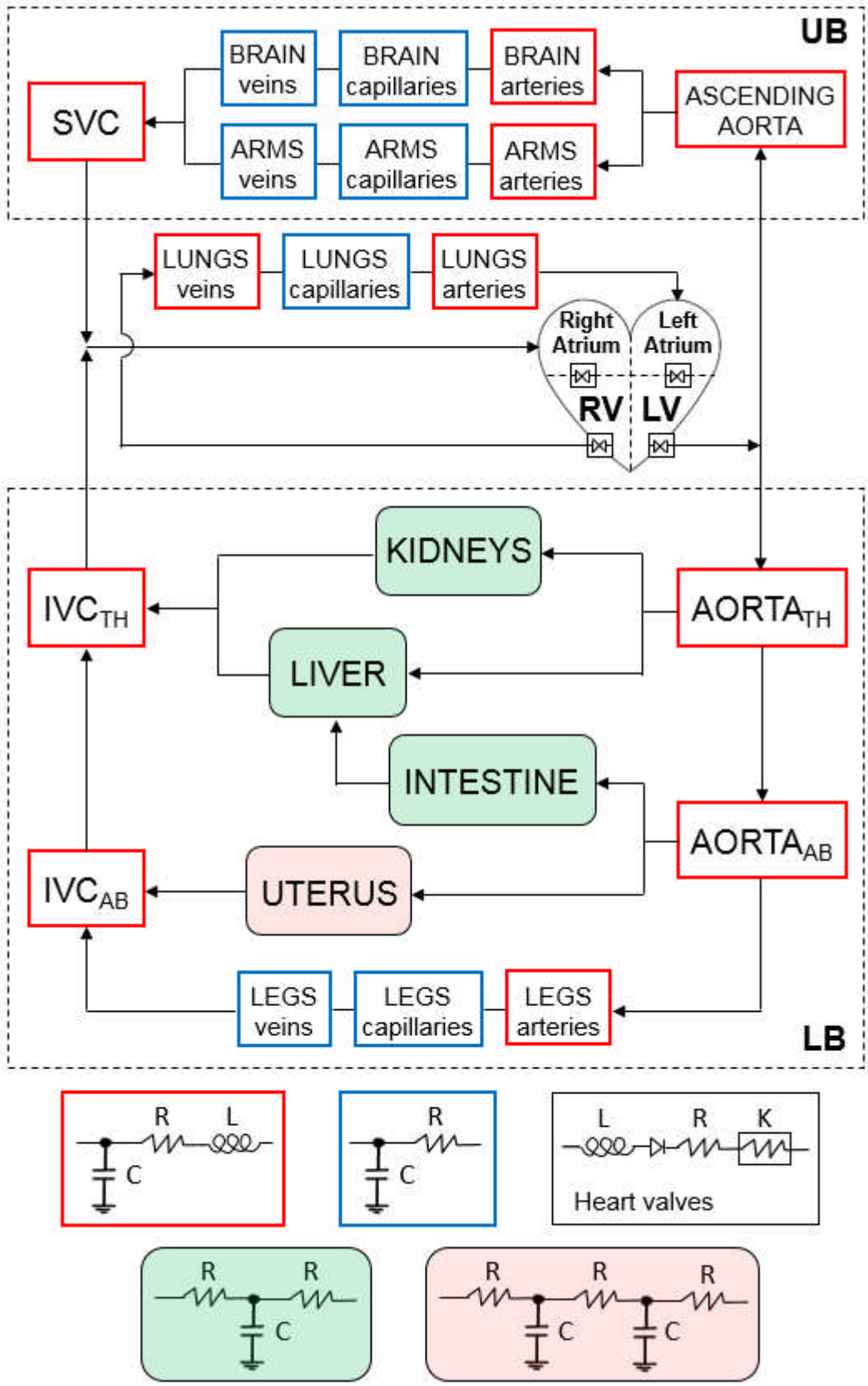
UB
BRAIN veins
BRAIN capillaries
BRAIN arteries
SVC
ASCENDING AORTA
ARMS veins
ARMS capillaries
ARMS arteries
LUNGS veins
LUNGS capillaries
LUNGS arteries
Right Atrium
Left Atrium
RV
LV
KIDNEYS
IVC$_{TH}$
AORTA$_{TH}$
LIVER
INTESTINE
AORTA$_{AB}$
IVC$_{AB}$
UTERUS
LEGS veins
LEGS capillaries
LEGS arteries
LB
R
L
C
R
C
L
R
K
Heart valves
R
R
C
R
R
R
C
C

688 **Figure 2**

689

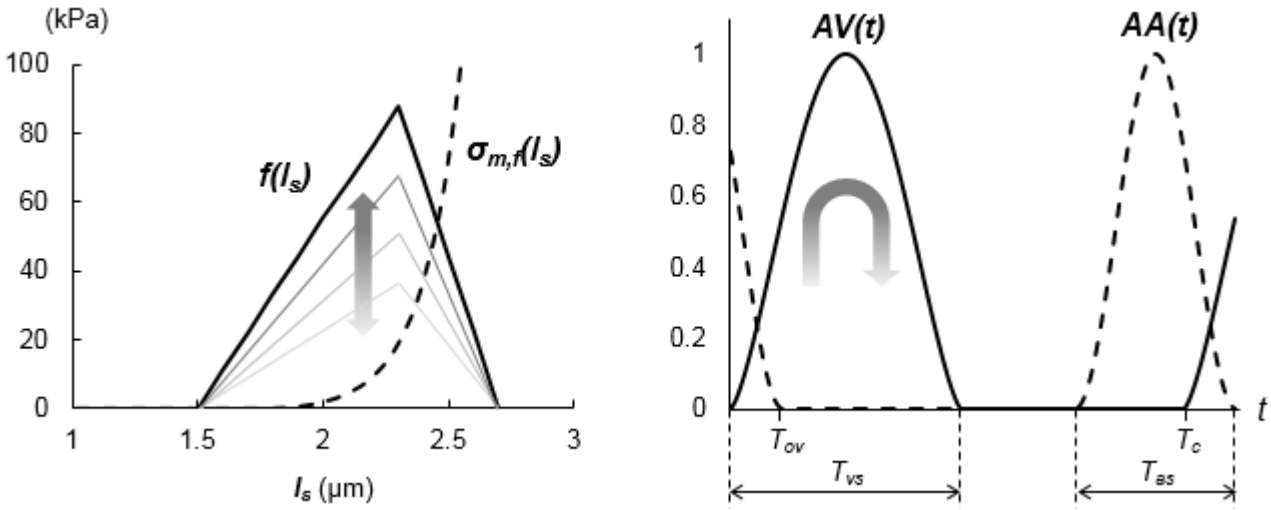

690

691

692 **Figure 3**

693

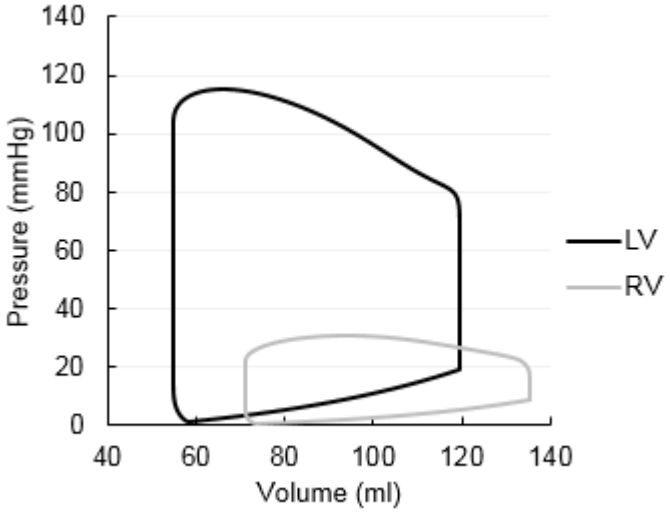

694

695

Figure 4

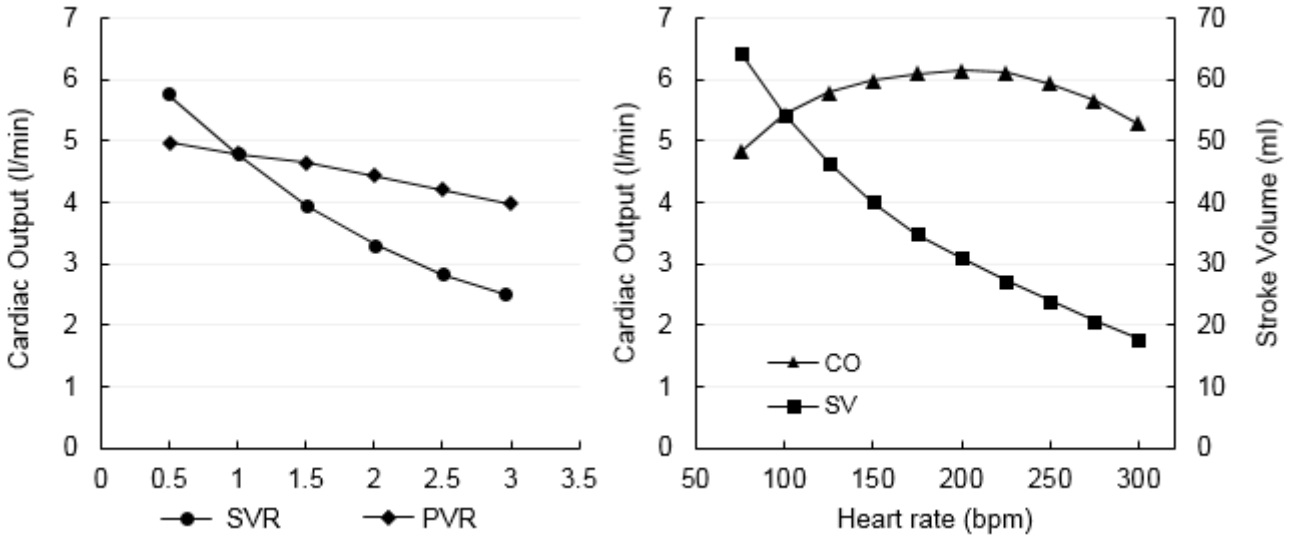
Cardiac Output (l/min)
0
1
2
3
4
5
6
7
0
0.5
1
1.5
2
2.5
3
3.5
SVR
PVR
Cardiac Output (l/min)
Stroke Volume (ml)
0
10
20
30
40
50
60
70
50
100
150
200
250
300
Heart rate (bpm)
CO
SV

700 **Figure 5**

701

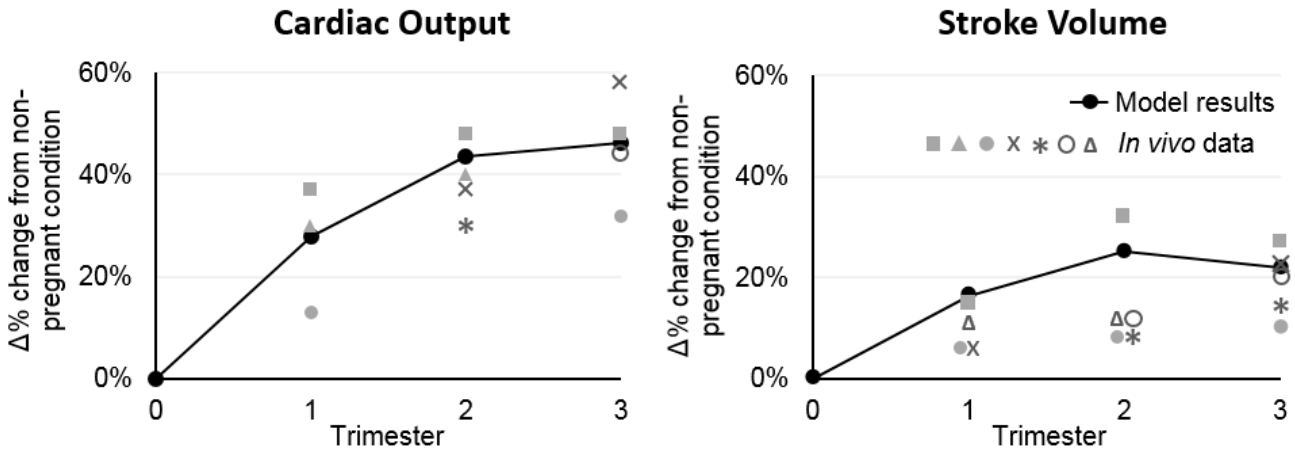

702

703

704 **Figure 6**

705

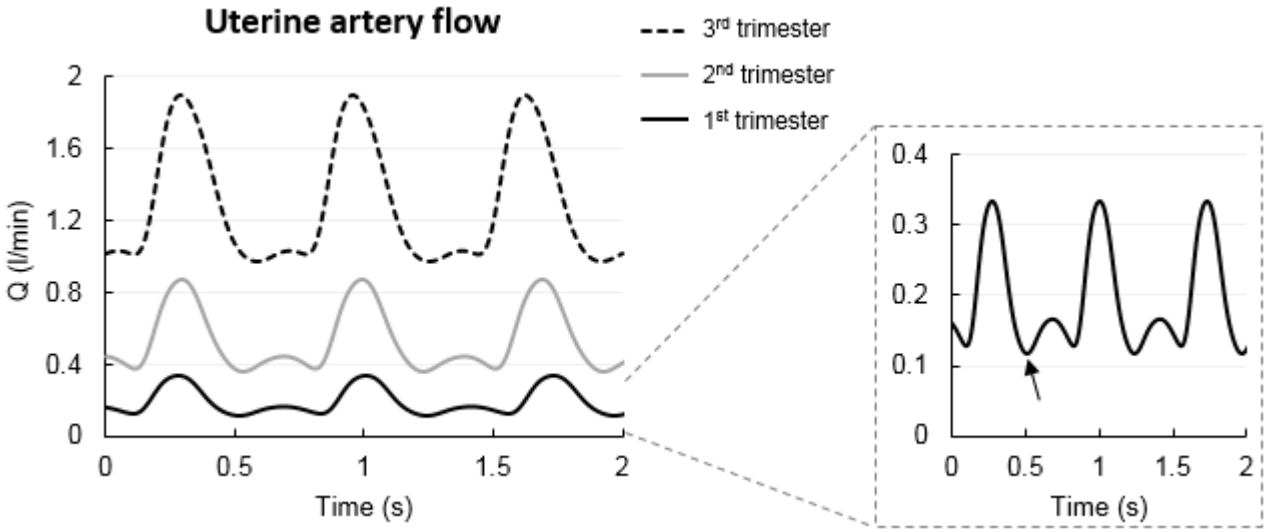

706

707